Mon. Not. R. Astron. Soc. **314**, 295–306 (2000)

Population synthesis of H II galaxies

D. Raimann,[1★] E. Bica,[1★] T. Storchi-Bergmann,[1★] J. Melnick[2★] and H. Schmitt[3★]
[1]*Universidade Federal do Rio Grande do Sul, IF, CP15051, Porto Alegre 91501-970, RS, Brazil*
[2]*European Southern Observatory, Casilla 19001, Santiago 19, Chile*
[3]*Space Telescope Institute, 3700 San Martin Drive, Baltimore, MD 21218, USA*

Accepted 1999 December 2. Received 1999 October 29; in original form 1999 August 23

ABSTRACT

We study the stellar population of galaxies with active star formation, determining ages of the stellar components by means of spectral population synthesis of their absorption spectra. The data consist of optical spectra of 185 nearby ($z \leqslant 0.075$) emission-line galaxies. They are mostly H II galaxies, but we also include some starbursts and Seyfert 2s, for comparison purposes. They were grouped into 19 high signal-to-noise ratio template spectra, according to their continuum distribution, absorption- and emission-line characteristics. The templates were then synthesized with a star cluster spectral base.

The synthesis results indicate that H II galaxies are typically age-composite stellar systems, presenting important contributions from generations up to as old as 500 Myr. We detect a significant contribution of populations with ages older than 1 Gyr in two groups of H II galaxies. The age distributions of stellar populations among starbursts can vary considerably despite similarities in the emission-line spectra. In the case of Seyfert 2 groups we obtain important contributions from the old population, consistent with a bulge.

From the diversity of star formation histories, we conclude that typical H II galaxies in the local Universe *are not* systems presently forming their first stellar generation.

Key words: H II regions – galaxies: compact – galaxies: evolution – galaxies: starburst – galaxies: stellar content.

1 INTRODUCTION

H II galaxies are gas-rich dwarf galaxies undergoing violent star formation characterized by an important population of massive stars with strong narrow emission lines (Melnick, Terlevich & Eggleton 1985; for a review see Melnick 1992). Their study began with the discovery by Sargent & Searle (1970) that some compact galaxies in Zwicky's Catalogue (1971) had spectra comparable to those of giant H II regions.

Many of these objects have a compact morphology with a dominant starbursting region, but some have double or multiple components (Telles, Melnick & Terlevich 1997). Terlevich et al. (1991) built a catalogue of H II galaxy spectra and analysed the properties of the individual objects, such as distributions of redshift, Balmer decrement, Hβ luminosity and equivalent width. In particular, they derived $-1.4 < [O/H] < -0.4$, showing that H II galaxies are typically metal deficient.

An important question is whether H II galaxies are young systems that are forming their first generation of stars, or systems that have multiple stellar generations, including several Gyr old ones. Several studies have searched for an underlying old stellar component but the results were not conclusive (Thuan 1983; Campbell & Terlevich 1984; Melnick et al. 1985; Farnell, O'Connel & Thuan 1988). It would also be worth probing whether non-ionizing blue stellar populations (20–500 Myr) occur and in what proportions.

Brinks & Klein (1988) found that one H II galaxy (II Zw 40) may indeed be a young system, recently formed by the interaction of two H I clouds. On the other hand, Schulte-Ladbeck & Crone (1998) resolved red giant stars in the blue compact dwarf galaxy VII Zw 403 with the *Hubble Space Telescope*, and concluded that it is not a young galaxy forming its first generation of stars, having an older underlying component. Indeed, such red giants could be related to an intermediate or old age component since the colour–magnitude diagram could not distinguish such low turn-offs.

The spectral study of stellar populations requires a high-enough signal-to-noise (S/N) ratio to clearly establish the continuum distribution and absorption lines. Averaging spectra of similar properties has proven to be a powerful tool for stellar population analyses of star clusters and galaxies (e.g. Bica 1988; Bonatto, Bica & Alloin 1995; Santos et al. 1995).

The population synthesis of galaxies using a base of star cluster spectra (Bica 1988) has provided information on population components in normal galaxies. The method employs a grid of star cluster spectral properties built as a function of age and metallicity

★ E-mail: raimann@if.ufrgs.br (DR); bica@if.ufrgs.br (EB); thaisa@if.ufrgs.br (TS-B); jmelnick@eso.org (JM); schmitt@stsci.edu (HS)

Table 1. The resulting spectral groups and their member galaxies.

Designation	Morphology/ Spectral types	z	M_B
G_Cam1148-2020 H II $1.5 \times 1.8\,\mathrm{kpc}^2$ $\langle M_B \rangle = -17.8 \pm 1.1$			
Cam1148-2020[a]	H II TI	0.012	
Cam0341-4045E[a]	H II TI	0.015	
Tol 1214-277	H II TI	0.026	−17.59
Tol 1008-286	H II E? TI	0.014	−19.31
Tol 1304-353	H II	0.014	−16.74
Tol 1334-326	H II TI	0.012	−17.61
Tol 1304-386	H II	0.014	
UM568	H II	0.048	
UM411	H II	0.040	
G_UM461 H II $0.2 \times 0.3\,\mathrm{kpc}^2$ $\langle M_B \rangle = -15.0 \pm 2.7$			
UM461	H II BCD/Irr TII	0.003	−13.53
UM309	H II SAB(s)m	0.004	−19.11
UM462NE	H II pec;BCD	0.004	
UM462SW	H II pec;BCD	0.003	
UM463	H II	0.004	−12.62
UM439	H II TII	0.004	−15.92
II Zw 40	H II BCD/Irr/merger TI	0.003	−14.92
Tol 1116-325	H II TII	0.002	−11.52
Tol 1400-411	H II IB(s)m	0.002	−17.32
G_Tol1924-416 H II blue $2.5 \times 3.3\,\mathrm{kpc}^2$ $\langle M_B \rangle = -20.0 \pm 0.9$			
Tol 1924-416	H II pec	0.009	−19.48
Cam1543+0907[a]		0.038	
Cam1409+1200[a]	TI	0.056	
Cam0357-3915[a]	H II TII	0.075	
Tol 1247-232	H II	0.048	−20.95
Tol 0513-393	H II TII	0.050	
Tol 1457-262b	H II	0.017	−19.46
G_NGC1487 H II $0.2 \times 0.3\,\mathrm{kpc}^2$ $\langle M_B \rangle = -17.1 \pm 1.1$			
NGC 1487a[a]	S pec (merger)	0.003	−18.00
NGC 1487b[a]	S pec (merger)	0.003	−18.00
NGC 1487c[a]	S pec (merger)	0.003	−18.00
Tol 0957-278	H II multiple system?	0.005	−17.13
UM523	H II Im pec	0.003	−16.2
UM038	H II Sc	0.004	−15.52
G_Mrk710 starburst $0.2 \times 0.4\,\mathrm{kpc}^2$ $\langle M_B \rangle = -18.5$			
Mrk710	H II SB(rs)ab	0.005	−18.47
UM506	H II	0.005	
G_Tol1004-296 H II $0.4 \times 0.6\,\mathrm{kpc}^2$ $\langle M_B \rangle = -17.2 \pm 1.2$			
Tol 1004-296NW	H II TII:	0.003	
Tol 1004-296SE	H II	0.004	
Tol 0633-415	H II TI	0.017	−17.65
Tol 1324-276	H II S? TII:	0.006	−17.46
Tol 1223-359	H II	0.009	−15.31
Fairall 30	H II SAB(r)0 TII	0.004	
Cam1148-2020B[a]	H II	0.012	
UM311	H II	0.006	
UM372	H II	0.005	
UM238	H II S TII	0.014	−17.18
UM382	H II	0.012	
UM626	H II	0.011	
UM619	H II Sm	0.015	−18.49
UM408	H II TII	0.018	
UM069W	H II	0.006	
UM133	H II TII	0.007	
UM505	H II	0.004	

Table 1 – *continued*

Designation	Morphology/ Spectral types	z	M_B
G_UM448 H II $1.8 \times 2.1\,\mathrm{kpc}^2$			
UM448	H II Sb pec TI	0.018	−19.46
G_Tol0440-381 H II $1.5 \times 2.7\,\mathrm{kpc}^2$ $\langle M_B \rangle = -18.6 \pm 0.7$			
Tol 0440-381	H II TI	0.041	
Tol 1025-284	H II TI:	0.032	−18.66
Tol 0645-376	H II TI	0.026	
Tol 1457-262f	H II	0.017	
Tol 0620-386	H II	0.067	
Cam0951-1733[a]		0.028	
UM653	H II Sy2	0.038	−17.91
UM469	H II	0.058	−18.83
UM254	H II Sy2	0.044	−19.23
UM471	H II	0.035	−17.00
UM401	H II	0.032	
UM031	H II	0.042	
UM628	H II	0.024	
UM377	H II	0.029	
UM410S	H II S	0.023	−18.82
UM410N	H II S	0.023	−18.82
UM048	H II S	0.016	−18.53
UM494	H II cIBm	0.028	−19.95
G_UM504 H II $0.4 \times 0.8\,\mathrm{kpc}^2$ $\langle M_B \rangle = -15.9 \pm 0.7$			
UM504	H II	0.007	−15.08
UM330	H II	0.017	
UM077	H II	0.017	−15.56
UM080	H II	0.016	−16.21
UM051	H II Sc	0.014	
UM323	H II BCD	0.006	−15.22
UM069E	H II	0.006	
UM069	H II	0.006	
UM513	H II	0.012	−15.88
UM491	H II	0.006	−15.29
UM040S	H II SB0?	0.004	−15.72
Cam0945-2219b[a]		0.015	
Tol 0527-394	H II	0.015	
Tol 1147-283	H II N TII	0.007	−16.33
Tol 1324-276nuc	H II S? TII:	0.006	−17.46
G_Cam0949-2126 H II/starb. $2.5 \times 3.8\,\mathrm{kpc}^2$ $\langle M_B \rangle = -19.7 \pm 1.5$			
Cam0949-2126[a]		0.028	
Tol 1457-262a	H II	0.017	
Tol 0336-407	H II	0.065	
Fairall 02	H II SB(r)a	0.055	−21.35
Cam0840+1201[a]	TI	0.030	−17.88
UM150	H II S	0.043	−19.18
UM307	H II Sdm:	0.023	−20.51
UM083	H II	0.040	
UM358	H II	0.056	

Table 1 – *continued*

Designation	Morphology/ Spectral types	z	M_B
G_UM71 H II $1.1 \times 2.1\,\mathrm{kpc}^2$ $\langle M_B \rangle = -17.7 \pm 1.2$			
UM71	H II	0.040	−19.52
UM441	H II	0.044	−19.09
UM061	H II Sc+	0.037	−18.85
UM047	H II	0.021	−18.62
UM065	H II	0.021	−17.42
UM017	H II	0.027	
UM227	H II Compact	0.030	−18.90
UM098	H II	0.023	
UM582	H II	0.058	
UM110	H II	0.030	−18.29
UM595	H II IR	0.021	−18.55
UM219	H II SBa	0.013	−17.08
UM354	H II	0.031	
UM390	H II	0.034	
UM151	H II Compact	0.016	−17.03
UM612	H II	0.015	
UM055	H II	0.018	
UM374	H II	0.019	
UM351	H II	0.026	−16.91
UM442	H II	0.027	−17.68
UM306	H II	0.016	−17.26
UM147	H II	0.032	
UM618	H II	0.014	
UM635	H II	0.025	
UM345	H II	0.019	
UM455	H II TII	0.012	−15.55
UM376	H II	0.039	
UM507	H II	0.020	−15.98
UM369	H II	0.019	
Fairall 05	H II Bright Nucleus	0.029	
Tol 0452-416	H II	0.037	
Cam0841-1610[a]		0.028	
Cam0954-1852SE[a]		0.014	
Cam0939-2107[a]		0.015	
Cam0952-2028[a]		0.028	
Tol 1345-420	H II TII	0.008	−16.23
G_NGC1510 H II $0.3 \times 0.4\,\mathrm{kpc}^2$			
NGC 1510[a]	SA0 pec H II	0.003	−16.93
G_Mrk711 H II/starb. $1.4 \times 2.1\,\mathrm{kpc}^2$ $\langle M_B \rangle = -19.8 \pm 0.8$			
Mrk711	H II Compact SB nuc.	0.019	−18.9
UM448W	H II Sb pec:	0.018	−19.59
Cam08-28A[a]	Compact TI	0.053	−20.93
Cam0942-1929a[a]		0.033	
UM623	H II	0.034	

Table 1 – *continued*

Designation	Morphology/ Spectral types	z	M_B
G_UM140 H II/starb. $0.8 \times 1.5\,\mathrm{kpc}^2 \langle M_B \rangle = -18.1 \pm 0.9$			
UM140	H II Compact	0.017	−19.03
UM054	H II	0.016	−18.44
UM622	H II	0.025	−19.50
UM033	H II	0.029	
UM119	H II	0.021	
UM395	H II S	0.022	−18.27
UM134	H II	0.018	
UM063	H II Sb	0.018	−17.29
UM064	H II	0.018	−17.29
UM079	H II	0.017	
UM049	H II	0.014	
Cam0956-2143[a]		0.016	
Cam0956-1916[a]		0.012	
UM512	H II	0.015	−17.32
UM371	H II	0.018	−17.64
G_NGC3089 H II/starb. $1.1 \times 2.1\,\mathrm{kpc}^2$ $\langle M_B \rangle = -19.3 \pm 1.0$			
NGC 3089[a]	SAB(rs)b	0.009	−19.57
Tol 1025-285	H II N	0.031	−19.30
UM308	H II S0: sp	0.016	−18.53
UM304	H II Sb	0.016	−19.03
UM027	H II	0.034	−19.92
UM646	H II	0.025	−18.65
UM598	H II SAB(s)b pec	0.022	−21.75
UM078	H II	0.040	−18.88
UM391	H II Compact	0.021	−19.22
UM203	H II	0.040	−18.02
UM601	H II	0.028	
G_UM477 starburst $0.7 \times 1.4\,\mathrm{kpc}^2$ $\langle M_B \rangle = -20.1 \pm 0.9$			
UM477	H II SB(r)c	0.004	−19.04
UM467	H II (R)SAB0+	0.019	−18.45
UM274	H II SA(rs)b pec?	0.013	−20.61
UM418	H II (R')SAB(s)b pec	0.026	−20.79
UM152E	H II Sc	0.018	−19.79
UM152W	H II SBm pec:	0.018	−20.38
UM093	H II Compact	0.032	−21.08
NGC 4536 nuc[a]	SAB(rs)bc H II	0.006	−20.74
G_UM103 Seyfert 2 $1.8 \times 3.7\,\mathrm{kpc}^2$ $\langle M_B \rangle = -19.7 \pm 0.4$			
UM103	Sy2	0.045	−19.28
NGC 2989[a]	SAB(s)bc:	0.014	−20.16
Tol 0514-415	Sy2	0.049	
G_NGC4507 Seyfert 2 $1.7 \times 3.5\,\mathrm{kpc}^2$ $\langle M_B \rangle = -19.8 \pm 0.8$			
NGC 4507[a]	SAB(s)ab Sy2	0.012	−20.49
NGC 3081[a]	(R_1)SAB(r)0/a Sy2	0.008	−19.67
UM082	Sy2	0.051	−18.67
UM363	Sy2 (R)SAB(rs)0+:	0.018	−20.61
UM085	Sy2	0.041	−18.78
UM293	Sy2 Sy1.5	0.056	−20.35
UM016	Sy2	0.058	−19.83
G_NGC3281 Seyfert 2 $1.2 \times 2.4\,\mathrm{kpc}^2$ $\langle M_B \rangle = -19.7 \pm 1.0$			
NGC 3281[a]	SAB(rs+)a Sy2	0.012	−20.71
NGC 1386[a]	SB(s)0+ Sy2	0.003	−18.31
UM319	Sy2 SB?	0.016	−19.15
UM105	Sy2	0.030	−20.21
Tol 0611-379	Sy2	0.038	
Tol 0544-395	Sy2 (R)AS(r)0/a	0.025	−20.10

[a] Additional galaxies with respect to Terlevich et al. (1991).

(Bica & Alloin 1986a,b). The synthesis provides flux fractions for the successive generations of star formation and corresponding chemical enrichment. The method was also applied to the dusty metal-rich starburst galaxy NGC 6240 (Schmitt, Bica & Pastoriza 1996). Recently, the algorithm was adapted to the ultraviolet (UV) range (Bonatto et al. 1998, 1999).

In this paper we use the star cluster synthesis method to investigate the stellar populations of H II galaxies and to compare them with those of more luminous emission-line galaxies such as starbursts and Seyfert 2s. We intend to shed light on the question of whether H II galaxies are single or multigeneration systems. We present the sample and spectral group construction in Section 2. The population syntheses are carried out and discussed in Section 3. The concluding remarks are given in Section 4. We defer consideration of the emission-line spectra to a forthcoming paper (Raimann et al. 2000, hereafter Paper II).

2 DATA

The data set consists of 185 emission-line galaxy spectra in the range $\lambda\lambda$3300–7000, with an average resolution of $\approx$5 Å. Most spectra (156) are a subsample of those obtained by Terlevich et al. (1991) for the spectrophotometric catalogue of H II galaxies and analyses of the emission properties of the individual objects. The present sample includes 29 additional objects, mostly starbursts and Seyfert 2 galaxies, obtained in the same observing runs. The selected spectra are those with enough continuum S/N ratio ($\approx$5–10) to allow one to distinguish the basic spectral distribution of the stellar population.

Prior to any spectral averaging among galaxies, individual spectra were corrected for the foreground (Milky Way) reddening (Burstein & Heiles 1984) using a normal reddening law (Seaton 1979). Subsequently, they were redshift corrected with radial velocities from Terlevich et al. (1991) or the NASA/IPAC Extragalactic Database (NED), or derived from the spectra themselves. Finally, the individual spectra were normalized to $F_\lambda = 10$ at $\lambda = 5870$ Å.

Many spectra had similar characteristics, allowing one to classify them into groups. We follow the spectral grouping procedures already applied to nuclear regions of early- and late-type normal galaxies (Bica 1988), and more recently to the UV range of early-type galaxies (Bonatto et al. 1996), nuclear starbursts of spiral galaxies (Bonatto et al. 1998) and star-forming galaxies in general (Bonatto et al. 1999). In the present study we considered the continuum spectral distribution, absorption features whenever seen (especially the Balmer jump), and emission lines. In the latter case we measured equivalent widths (W_λ) of the strongest emission lines [O II]λ3727, Hβ, [O III]λ4959 (and assuming a ratio of 1:3 we inferred the λ5007 line, thus avoiding any saturation effect), Hα and [N II]λ6584. In addition to spectral properties we adopted as grouping criteria comparable absolute magnitudes (M_B) and Hβ emission-line luminosities.

The criteria above, together with information on spectral (H II, starburst or Seyfert 2) and/or morphological (spiral, irregular, blue contact dwarf (BCD), interacting, etc.) characteristics, basically preclude that differently evolved galaxies be mixed in a given group. The sources for Hβ fluxes, *B*-integrated magnitudes, morphological and spectral types were Terlevich et al. (1991), the NED data base and Sandage & Tammann (1981). The spectral averages were weighted according to the continuum S/N ratio of the individual spectra. Finally, we point out that each averaging stage among galaxy spectra improved the S/N ratio, and these partial results were checked for compatibility before further averaging.

The resulting 19 spectral groups with their members are presented in Table 1. By columns: (1) galaxy designation, (2) morphological and/or spectral types, (3) redshift and (4) absolute magnitude (M_B) assuming $H_0 = 75\,\mathrm{km\,s^{-1}\,Mpc^{-1}}$. Each group in the table is named after the member galaxy with the best S/N ratio, and we also present in the table basic group characteristics, namely emission-line classification, average observed region ($\mathrm{kpc^2}$) corresponding to the employed slit and the respective galaxy redshift, and finally average absolute magnitude ($\langle M_B \rangle$).

We emphasize that the absolute magnitudes in Table 1 are indicative since the sources of *B* magnitudes are heterogeneous, varying from photographic estimates in surveys and detailed photographic analyses for bright galaxies to charged-coupled device (CCD) imaging analyses. In some cases (e.g. NGC 1487) the extensions in column 1 indicate clumps in the same object, so we adopted the absolute magnitude of the ensemble galaxy (column 4). Depending on the radial velocities within each group the basic spatial region observed varies from 0.2×0.3 to $2.5 \times 3.8\,\mathrm{kpc^2}$ with an average value of $1.1 \times 1.9\,\mathrm{kpc^2}$.

Note that we are typically dealing with compact sources; in many cases they are nearly stellar in survey plates (e.g. the UM Catalogue: MacAlpine, Smith & Lewis 1977). Deep CCD imaging of H II galaxies and structural analyses are available for relatively small samples (e.g. Telles & Terlevich 1997; Telles et al. 1997). In particular, Telles et al. (1997) classify H II galaxies into Type I which are more disturbed and extended having larger luminosities and velocity dispersions, and more compact and regular Type II objects. We also recall in column 2 this classification. Note that G_Tol1004-296 has a significant number of galaxies in common with Telles et al. (1997) being typically of Type II, while G_Cam1148-2020 has five galaxies in common, all of Type I. The morphological/spectral information in Table 1 is also interesting to see how often galaxies in each group have been classified as H II (most groups), how in certain groups spiral morphology is mentioned with peculiarities that could suggest the starburst phenomenon (e.g. G_UM477), and finally other groups wherein Seyfert 2s are mentioned (e.g. G_NGC4507).

2.1 The spectral groups

The resulting spectral group templates are shown in Fig. 1, where the nature of the emission-line component is also indicated. They can be basically inferred from information on member galaxies in Table 1. However, for the sake of clarity what we show in Fig. 1 as emission classification is a high-precision a posteriori result (Paper II). It is based on the distribution of emission-line spectra of the groups in the Baldwin, Phillips & Terlevich (1981) diagnostic diagram, after subtraction of stellar population models. In addition to the classifications as H II galaxies, starbursts and Seyfert 2s, we give intermediate H II/starburst classification for groups near this bordering locus in the diagnostic diagram.

The groups are ordered from bluer to redder continuum distributions in the figure. Note that most H II groups have indeed very blue continua as expected from stellar populations dominated by very recent star formation, but some H II groups have a prominent Balmer jump in absorption, suggesting the presence of evolved blue stellar populations. The intermediate H II/starburst groups sit on stellar populations with a Balmer jump in absorption and in some cases (e.g. G_UM140) with an incipient 4000-Å

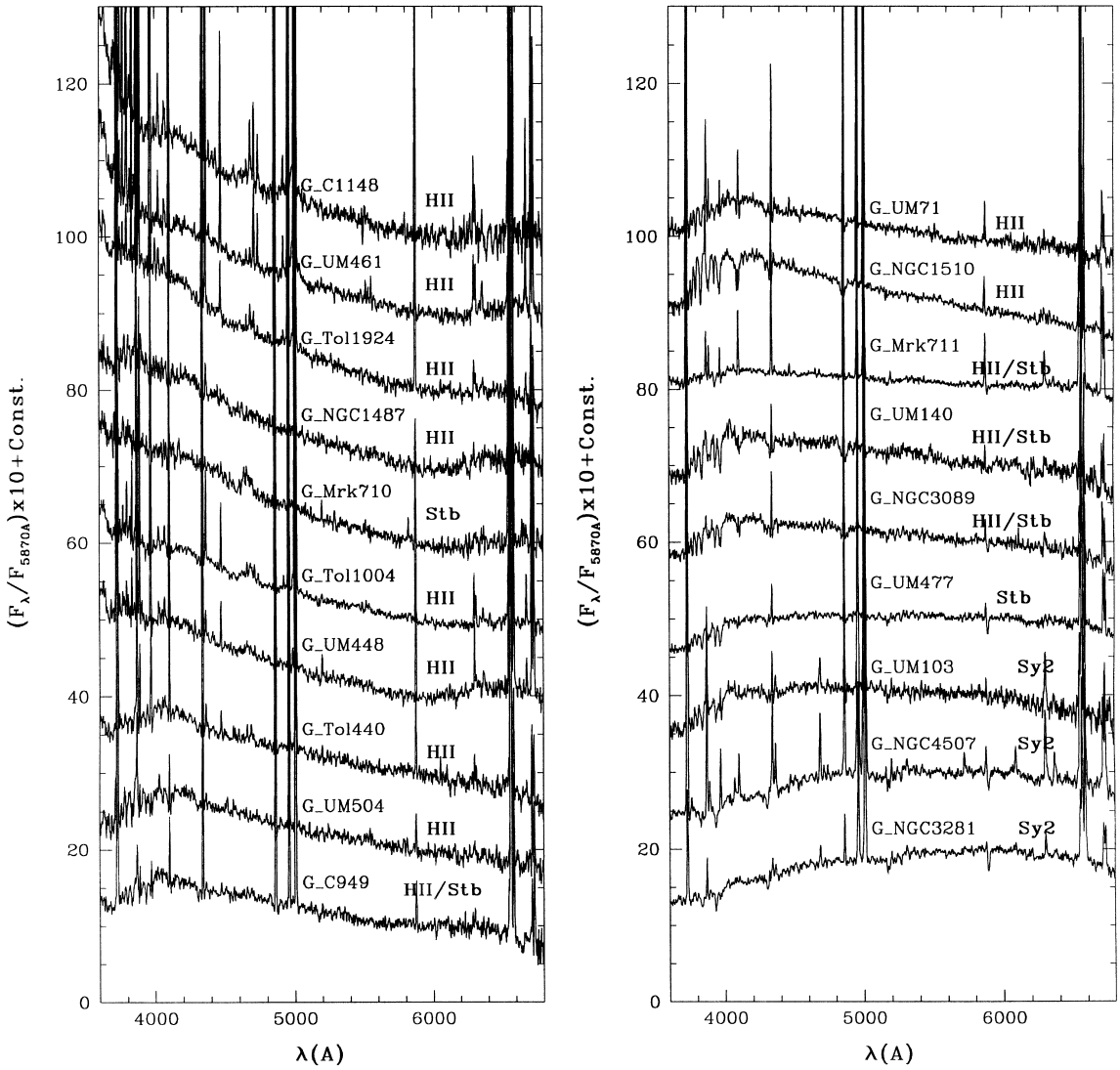

Figure 1. The resulting spectral group templates. The basic emission-line natures of the groups as H II galaxy, intermediate H II/starburst, starburst and Seyfert 2 are indicated. For some groups, designations are abbreviated.

break which is a characteristic of populations older than 1 Gyr. For a detailed discussion of the Balmer jump and 4000-Å break as a function of age and metallicity in single-age stellar populations, see Bica, Alloin & Schmitt (1994). One starburst group is very blue (G_Mrk710), while the other (G_UM477) has a 4000-Å break, suggesting an important intermediate age ($1 < t < 9$ Gyr) and/or old ($t > 10$ Gyr) metal-rich components. We can add to the starburst variety of stellar populations very steep spectra rising towards the infrared, such as that of NGC 6240 wherein dust absorption considerably affects both recent star formation and the bulge stellar population, as unveiled in the synthesis by Schmitt et al. (1996). Two Seyfert 2 groups are very red, while one (G_UM103) is somewhat bluer. Finally, note that some very blue H II groups and one starburst group (G_Mrk710) present the wide Wolf–Rayet feature at $\lambda \approx 4680$ Å.

3 POPULATION SYNTHESES

The star cluster method to synthesize galaxy spectra (Bica 1988) reduces the number of variables to age and metallicity. The synthesized quantities are W_λ of the main absorption spectral features and continuum fluxes (F_λ). These quantities are measured in each spectrum and are compared with combinations of the base elements which in turn have known ages and metallicities. An algorithm generates these combinations in a selected step and compares the synthesized W_λ and F_λ with the observed values. The possible solutions are those that reproduce, within allowed limits, the observed W_λ and F_λ of the galaxy spectrum. The results obtained through this method are percentage flux fractions (at a selected wavelength) of the different age and metallicity components.

The algorithm used is an upgraded version (Schmitt et al. 1996). It is faster than previous versions and also solves for the internal reddening $E(B-V)_i$ that affects the stellar population.

The employed W_λ were those of K Ca II (corresponding to the spectral window $\lambda\lambda$3908–3952), CN-band ($\lambda\lambda$4150–4214), G-band ($\lambda\lambda$4284–4318) and Mg I ($\lambda\lambda$5156–5196). The continuum fluxes were measured at $\lambda = 3660$, 4020, 4510 and 6630 Å, normalized at $\lambda = 5870$ Å. Table 2 shows these quantities for the 19 groups.

We point out that for the spectral groups within the stellar population range of galaxy spectra discussed in Bica (1988) we employed essentially the same component base, whereas for bluer

Table 2. Absorption-line equivalent widths and F_λ relative continuum fluxes for the spectral groups.

Group	W(K Ca II)	W(CN-band)	W(G-band)	W(Mg I)	$\frac{F_{3660}}{F_{5870}}$	$\frac{F_{4020}}{F_{5870}}$	$\frac{F_{4510}}{F_{5870}}$	$\frac{F_{6630}}{F_{5870}}$
G_Cam1148-2020	−0.2	−0.3	0.0	−0.1	3.33	2.27	1.72	1.09
G_UM461	0.7	−1.9	−0.7	0.8	3.03	2.21	1.77	1.07
G_Tol1924-416	1.0	−0.7	0.7	1.0	2.64	2.42	1.76	0.86
G_NGC1487	1.0	0.2	0.0	0.7	2.34	2.28	1.79	1.17
G_Tol1004-296	2.1	−1.2	0.1	0.0	2.23	1.97	1.62	0.94
G_UM448	2.1	−2.5	−0.8	2.3	2.01	1.90	1.58	1.10
G_Tol0440-381	1.3	−1.0	1.4	1.1	1.58	1.78	1.43	0.69
G_UM504	2.1	−0.3	2.3	2.5	1.40	1.70	1.48	0.79
G_UM71	2.9	−0.5	2.3	1.9	1.10	1.53	1.34	0.74
G_NGC1510	3.0	0.1	1.4	2.2	1.06	1.72	1.58	0.79
G_Cam0949-2126	4.0	3.3	3.7	3.4	1.26	1.66	1.42	0.75
G_Mrk711	3.7	−0.8	1.3	2.1	1.06	1.20	1.14	0.97
G_UM140	2.2	1.1	1.9	3.7	0.86	1.35	1.31	0.80
G_NGC3089	2.5	0.1	3.0	2.8	0.82	1.30	1.19	0.81
G_Mrk710	1.5	−1.6	0.1	1.1	2.31	2.06	1.77	0.95
G_UM477	2.6	−0.5	2.3	3.7	0.60	0.91	1.04	0.90
G_UM103	5.3	3.3	4.1	2.6	0.59	1.07	1.11	0.72
G_NGC4507	13.7	7.6	7.6	5.7	0.49	0.66	0.88	0.84
G_NGC3281	13.6	5.6	6.7	6.5	0.35	0.56	0.77	0.83

Note. W_λ in Å.

Table 3. Base II properties.

Age (Myr)	Template	W(K Ca II)	W(CN-band)	W(G-band)	W(Mg I)	$\frac{F_{3660}}{F_{4020}}$	$\frac{F_{3780}}{F_{4020}}$	$\frac{F_{4510}}{F_{4020}}$	$\frac{F_{5313}}{F_{4020}}$
2–3	H IIy.LMC[a]	0.00	0.00	0.00	0.00	1.60	1.40	0.80	0.5
3–5A	H IIo.LMC[a]	0.00	0.00	0.00	0.00	1.50	1.20	0.73	0.5
3–5B	YA_SG.LMC[a]	2.10	2.90	1.10	1.20	1.06	1.12	0.79	0.55
6–9	YB.LMC[a]	0.99	0.58	1.23	1.31	0.67	0.80	0.80	0.57
12–40	YC.LMC[a]	1.87	0.48	0.42	0.15	0.67	0.94	0.75	0.53
35–65	YDE.LMC[a]	2.60	0.82	0.67	0.78	0.52	0.89	0.79	0.51
100	Y3[b]	3.80	2.20	1.20	2.50	0.51	0.76	0.78	0.65
500	Y4[b]	9.20	6.10	4.40	4.50	0.50	0.66	0.91	0.83
10 000	G1[b]	17.30	12.0	9.30	7.40	0.65	0.67	1.42	1.72

[a] Template in Santos et al. (1991).
[b] Template in Bica (1988).

spectral groups (Section 3.2) we adopted a new base with higher time resolution for young components. In the following discussions we will refer to them as Bases I and II, respectively.

Base I consists of the W_λ and F_λ values given by Bica & Alloin (1986b) for single-age stellar populations in the age range from H II regions to globular clusters and metallicities $0.6 \geqslant [Z/Z_\odot] \geqslant -2.0$. For the H II region element we used new values: $F_{3660}/F_{5870} = 3.28$, $F_{4020}/F_{5870} = 2.20$, $F_{4510}/F_{5870} = 1.73$ and $F_{6630}/F_{5870} = 0.74$ which are based on a larger number of observed H II regions.

Base II consists of the W_λ and F_λ values derived from the spectral observations of star clusters of the Large Magellanic Cloud (LMC), and derived templates (Santos et al. 1995). These templates have subsolar metallicity ([Fe/H] ≈ 0.5) which is suitable for H II galaxies, and have ages in the range 2–65 Myr. We complemented them with some elements from Base I ($t = 100, 500$ Myr and 10 Gyr). Base II is presented in Table 3. This new base has a normalization wavelength at $\lambda = 4020$ Å, because the spectra have a spectral range $\lambda\lambda 3600$–5500, thus not reaching the previous normalization wavelength $\lambda = 5870$ Å. More details on the implementation of Base II in the synthesis algorithm are given in Raimann (1998).

We point out that, in all present spectra, emission lines are strong and Balmer lines as a rule have both absorption and emission components. We do not use Balmer lines in the syntheses. However, metal lines in the blue–visible range like K Ca II and Mg I are fiducial age constraints because of dilution effects (Bica 1988), capable of indicating the presence and amount of intermediate age and/or old components.

3.1 Groups synthesized with Base I

Following Bica (1988) and Schmitt et al. (1996), the first synthesis step is to map out the possible solution space in the plane $t \times [Z/Z_\odot]$ which provides an indication of the enrichment level attained by the stellar population components. Dominant components are identified, which helps to constrain an evolutionary path in the plane. Subsequently syntheses were performed using a selected path. Paths 1–3 attain metallicities of $[Z/Z_\odot] = 0.0$, +0.3 and +0.6, respectively, for the intermediate age and young components. In the old bin (10 Gyr) the paths span from $[Z/Z_\odot] = -2.0$ up to the respective upper level above. For a visualization of such evolutionary paths in the plane metallicity versus age, see Bica (1988).

For each synthesis we probe possible internal reddening values affecting the stellar population as a whole. They are in the range $0 \leqslant E(B-V)_i \leqslant 0.50$ with 0.02 as step. The contribution of each base component (flux fractions at 5870 Å) varies from 0 to 100 per cent, initially with a step of 10 per cent. In this stage we test the allowed limits of each feature equivalent width and continuum point.

Table 4. Groups synthesized with Base I: percentage contribution to $F_{\lambda 5870}$.

Group	Path	3 Myr	10 Myr	50 Myr	100 Myr	500 Myr	1 Gyr	5 Gyr	10 Gyr +0.3[a]	10 Gyr 0.0[a]	10 Gyr <0.0[a]	$E(B-V)_{\rm i}$
G_UM504	2	24	2	14	41	5	2	1	1	1	9	0.02
G_UM71	1	15	0	0	51	12	1	1		1	19	0.02
G_NGC1510	1	9	1	23	59	2	1	1		0	4	0.01
G_Cam0949-2126	2	18	2	16	38	9	3	2	1	2	9	0.01
G_Mrk711	1	23	13	16	13	4	2	2		2	25	0.18
G_UM140	1	10	0	1	57	4	1	2		7	18	0.00
G_NGC3089	1	8	1	14	35	0	1	2		6	33	0.06
G_UM477	1	11	1	4	56	3	2	2		8	13	0.30
G_UM103	2	0	0	1	28	12	1	2	4	5	47	0.04
G_NGC4507	2	1	1	1	1	2	6	9	19	18	42	0.05
G_NGC3281	2	0	0	0	0	0	0	0	24	23	53	0.00

[a] Metallicity $[Z/Z_{\odot}]$.

Table 5. Groups synthesized with Base I: residuals.

Group	$\delta_{W(\rm K\ Ca\ II)}$	$\delta_{W(\rm CN\text{-}band)}$	$\delta_{W(G\text{-band})}$	$\delta_{W(\rm Mg\ I)}$	$\delta_{\frac{F_{3660}}{F_{5870}}}$	$\delta_{\frac{F_{4020}}{F_{5870}}}$	$\delta_{\frac{F_{4510}}{F_{5870}}}$	$\delta_{\frac{F_{6630}}{F_{5870}}}$
G_UM504	−1.5	−2.6	0.8	0.1	−0.01	−0.01	0.03	−0.04
G_UM71	−1.1	−2.7	0.6	−0.4	−0.08	−0.09	−0.06	−0.10
G_NGC1510	−0.6	−2.0	0.1	−0.2	−0.01	−0.07	0.09	−0.04
G_Cam0949-2126	−0.3	0.4	1.9	0.6	0.00	0.01	0.01	−0.09
G_Mrk711	−0.7	−2.7	−0.9	0.1	0.00	0.01	0.03	0.04
G_UM140	−2.3	−1.7	−0.1	0.8	0.00	−0.05	0.05	−0.08
G_NGC3089	−2.1	−2.5	0.8	0.1	−0.01	0.00	−0.01	−0.09
G_UM477	−1.7	−3.1	0.3	0.9	−0.05	−0.14	0.05	−0.07
G_UM103	−1.6	−0.6	0.7	−0.8	−0.05	−0.02	0.03	−0.19
G_NGC4507	1.3	−0.6	0.7	−0.1	0.02	−0.03	0.03	−0.14
G_NGC3281	−0.2	−2.9	−0.9	0.6	−0.08	−0.05	−0.05	−0.15

Finally, we run the synthesis algorithm with a step of 5 per cent for the base components. For the present galaxy spectra only paths 1 and 2 gave solutions. For each reddening value Path 1 (12 components) tests about 80×10^6 combinations, and by considering all reddening values it tests 2×10^9 combinations. Typically we find 200 000 solutions, which implies that 1 out of 10 000 combinations is a solution. For Path 2 (13 components) 5×10^9 combinations are tested and typically 10^6 solutions satisfy the allowed limits, implying a 1:5000 solution-to-combination ratio.

The synthesis results for the groups are presented in Table 4 in the form of percentage flux contribution from each age and metallicity component to the light at $\lambda = 5870$ Å. These flux fractions are averages of all solutions found. As in previous syntheses (e.g. Bica 1988; Bonatto et al. 1998, 1999) these values vary within 10 per cent among most solutions. The flux fractions are to be taken as probabilities of the presence of the respective component, and values smaller than 5 per cent must be taken with care. The last column shows the internal reddening $E(B-V)_{\rm i}$ affecting the stellar population obtained from the synthesis. The rms of reddening values among the solutions is typically $\sigma[E(B-V)_{\rm i}] = 0.03$.

The synthesis residuals (δ = observed-synthesized) for W_λ and continuum points are in Table 5. The residuals are usually $\leqslant 2$ Å for the W_λ and $\leqslant 0.05$ for the continua.

An illustration of synthesis with Base I is presented in Fig. 2, which shows the dereddened spectrum of the intermediate H II/starburst group G_NGC3089 [using the $E(B-V)_{\rm i}$ from Table 4], together with the synthesized spectrum constructed by the sum of the base spectra according to the proportions obtained from the synthesis (Table 4). We also provide component spectra grouped by age ranges, shown in relative proportions according to the synthesis.

We point out that the synthetic spectra are built with components which are available template spectra, associated as much as possible with grid elements, which are in turn those effectively used in the synthesis calculations. Note that, both in the grid and in the template spectrum, the H II region element (3 Myr) is a featureless continuum derived from an average of real H II regions. This featureless continuum is shown as a component in Fig. 2. Comparing the synthesized spectrum with the galaxy group spectrum (Fig. 2), the importance of the underlying stellar population absorptions to the study of the emission lines is clear. It can be seen the effect of Na I λ5893 absorption at the edge of He I λ5876 in emission. The lines Hβ λ4861 and Hγ λ4340 appear in emission despite the important underlying absorption. Finally, Hδ λ4102, Hε λ3970 and Hζ λ3889 are seen in absorption, but the synthesis indicates that they must be partially filled by their emission components. On the other hand, Hε has a contribution of [Ne III] λ3968 and an absorption contribution of H Ca II, since K Ca II λ3933 is present. In Paper II we will study the pure emission-line spectra after subtraction of the present absorption model spectra.

3.1.1 *Results*

The H II groups G_UM71 and G_UM504, the intermediate H II/starburst groups G_Cam0949-2126, G_UM140, G_Mrk711 and G_NGC3089, and the starburst group G_UM477 have an old stellar population contributing with about 10–40 per cent of the total flux at $\lambda = 5870$ Å. All these groups despite the strong emission lines are evolved galaxies dating back from the early Universe. These groups have a flux excess at $t \approx 100$ Myr, indicating a burst of star formation, except G_Mrk711 where flux fractions are more evenly distributed among age components.

G_NGC1510 (H II) has a marginally detected old component (less than 5 per cent of the total flux at $\lambda = 5870$ Å). It presents a

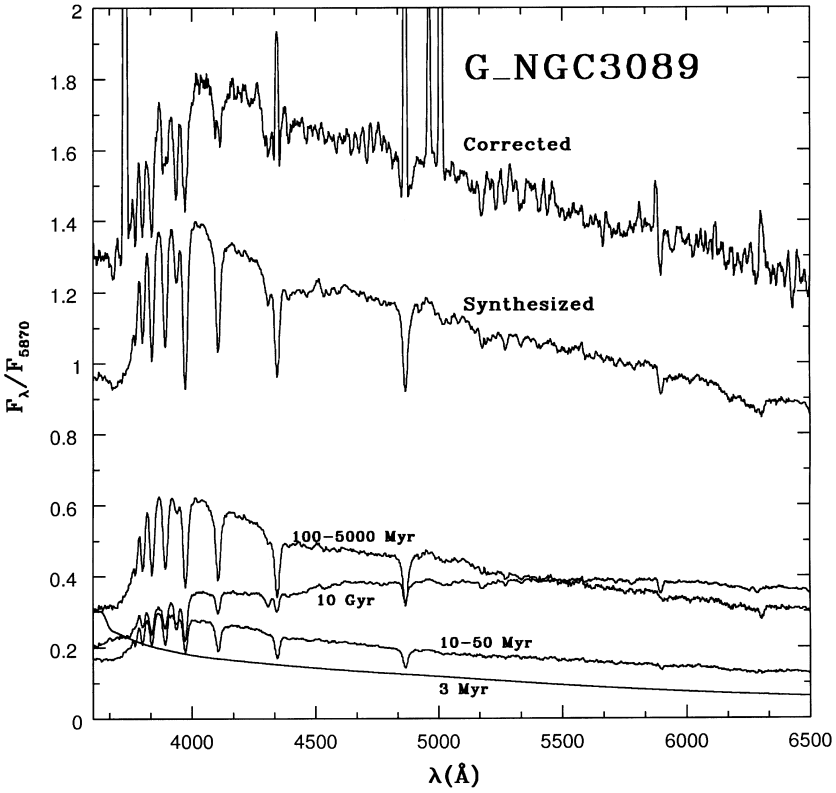

Figure 2. Spectrum of the group G_NGC3089 corrected for reddening $E(B-V)_{\rm i}$, the synthesized spectrum, and synthetic component spectra grouped by age ranges. The reddening-corrected spectrum has been shifted by a constant $C = +0.4$ for clarity.

burst around 100 Myr, contributing with almost 60 per cent of the total flux at $\lambda = 5870$ Å.

Seyfert 2 galaxies may contain some contribution of a featureless continuum in the near-UV. However, recent studies of the stellar population in Seyfert 2s (some of them in common with the present study) show that the featureless continuum (or combined with the H II region continuum) contribution amounts to less than 10 per cent at ≈3700 Å (Cid Fernandes, Storchi-Bergmann & Schmitt 1998; Storchi-Bergmann, Cid Fernandes & Schmitt 1998; Schmitt, Storchi-Bergmann & Cid Fernandes 1999). In the present cases such a contribution, if any, cannot be distinguished from that of H II regions.

The Seyfert 2 groups G_NGC3281, G_NGC4507 and G_UM103 have a dominant old stellar population (Table 4). They include most galaxies with late morphological type, in agreement with the strong old component which is characteristic of bulges. However, group G_UM103 has an additional burst of star formation with age $t \approx 100$ Myr contributing with ≈27 per cent of the total flux at $\lambda = 5870$ Å. This confirms previous results that Seyfert 2 nuclei can either sit on typical old bulge populations or include in the surroundings star-forming regions or evolved bursts of star formation. Indeed, Storchi-Bergmann, Bica & Pastoriza (1990) found this effect on scales of 2–5 kpc around the nucleus, while Cid Fernandes et al. (1998), Storchi-Bergmann et al. (1998) and Schmitt et al. (1999) found them in spatially resolved regions much closer to the nucleus.

We find a low internal reddening (column 13 of Table 4) for the Seyfert 2 groups. The same occurs for the other groups, except the intermediate H II/starburst group G_Mrk711 and the starburst group G_UM477 which have important reddening $E(B-V)_{\rm i} = 0.18$ and 0.30, respectively.

In column 2 of Table 4 we indicate the path that best describes the chemical enrichment. Most groups (especially H IIs) are described by a solar path (Path 1), but some (especially Seyfert 2s) follow the slightly more metal-rich Path 2.

Finally, it is interesting that on the average the contribution of old populations increases from the H II groups synthesizable with Base I to the intermediate H II/starburst groups. This suggests that we are dealing with a sequence of increasingly evolved galaxies.

3.2 Groups synthesized with Base II

The six elements coming from the spectral templates in Santos et al. (1995) are H IIy.LMC, H IIo.LMC, YA_SG.LMC, YB.LMC, YC.LMC and YDE.LMC. Note that the first (younger) and second elements are H II regions with underlying star clusters in two different evolutionary stages, and we treat them as featureless continua. The YA_SG.LMC template is a frequent spectral type among LMC clusters. It has essentially the same age range as the H IIo.LMC template, but it differs from the latter template by having an important contribution of hot supergiants and is basically emission free, possibly as a result of winds (Santos et al. 1995). The three remaining templates are the subsequent evolutionary stages of star clusters spanning the range 6–65 Myr. The template W_λ and continuum points are in Table 3.

Note that the present galaxy groups are extremely blue and not much flux from red stellar population components is expected. So we simply employed a red element of 10 Gyr which could in fact represent any intermediate age ($t > 1$ Gyr) or old component. The continuum points renormalized to $\lambda = 4020$ Å for the bluer groups, which are the subject of syntheses with Base II, are given in Table 6. We recall that the respective W_λ are in Table 2.

As for Base I we test the possibility of internal reddening $0 \leqslant E(B-V)_{\rm i} \leqslant 0.50$ with a 0.02 step. Base II has nine components which total about 75×10^6 combinations with a 5 per cent step for the flux fractions. Typically we obtain 4000 solutions which implies a solution-to-combination ratio of 1:18 750.

The synthesis results for these groups are presented in Table 7 and the residuals in Table 8. As an example, Fig. 3 shows the dereddened group G_Tol1004-296 according to the synthesis, the corresponding synthesis model and component spectra being grouped by age ranges. The underlying stellar population affects the emission-line spectrum less compared with the example given in Fig. 2.

It is worth remarking that the spectral boundary between the bluer and redder galaxy groups occurs for G_Tol0440-381 (synthesized with Base II) and G_UM504 (with Base I). Although there is no apparent colour break at this boundary (Fig. 1), the spectral properties of G_Tol0440-381 cannot be described by combinations of elements in Base I. A comparison of the synthesis results between G_Tol0440-381 (Table 7) and G_UM504 (Table 4) considering equivalent age ranges can be used to test the continuity of the syntheses for the two bases. The populations related to emission contribute with 33 and 24 per cent, respectively, while the blue star cluster components ($6 \leqslant t \leqslant 500$ Myr) have 66 and 62 per cent, respectively, and thus similar results. The old populations contribute with 1 and 11 per cent, respectively, which is at the limit of the significance level (Section 3.1). Indeed, the W_λ and F_λ measurements (Table 2) show significant differences between these two groups, in agreement with a population of slightly later type for G_UM504.

Table 6. F_λ continuum fluxes relative to F_{4020}.

Group	$\frac{F_{3660}}{F_{4020}}$	$\frac{F_{3780}}{F_{4020}}$	$\frac{F_{4510}}{F_{4020}}$	$\frac{F_{5313}}{F_{4020}}$
G_Cam1148-2020	1.43	1.14	0.75	0.54
G_UM461	1.38	1.14	0.80	0.58
G_Tol1924-416	1.11	1.09	0.72	0.51
G_NGC1487	1.03	1.09	0.80	0.56
G_Tol1004-296	1.14	1.03	0.80	0.57
G_UM448	1.07	1.12	0.82	0.62
G_Tol0440-381	0.85	0.87	0.79	0.63
G_Mrk710	1.08	1.11	0.84	0.55

3.2.1 *Results*

Most blue groups are dominated by components younger than 5 Myr, which is consistent with the fact that they have very strong emission-line spectra (Fig. 1). Note, however, that these groups are not single aged, because important flux fractions often occur to ages as old as 100 Myr. Finally, we point out that no red stellar population is allowed by the synthesis for most of these groups. Three groups (especially G_Tol1924-416) show a marginal detection, but at such levels the red component could represent any stellar population in the range $1 \leqslant t \leqslant 10$ Gyr. The internal reddening affecting the stellar populations $[E(B-V)_{\rm i}]$ is low, with the higher value $E(B-V)_{\rm i} = 0.16$ for to G_UM448.

3.3 Wolf–Rayet feature

The broad $\lambda\lambda$4650–4690 feature, arising in the atmospheres of Wolf–Rayet stars, is present in most of the bluer sample spectra (Fig. 1): the H II groups G_Cam1148-2020, G_Tol1004-296, G_UM448, G_Tol1924-416, G_UM461 and G_Tol0440-381, and the starburst group G_Mrk710. A blowup of the spectral region is shown for G_Cam1148-2020 in Fig. 4. Wolf–Rayet stars are highly evolved products of the evolution of massive stars ($M > 35\,{\rm M}_\odot$; see, e.g., Conti et al. 1983; Humphreys, Nichols & Massey 1985). Because of the limited age range in which they arise, Wolf–Rayet stars can be used as an age indicator in integrated spectra of star clusters (Santos et al. 1995 and references therein). Schaerer, Contini & Kunth (1999) studied Wolf–Rayet galaxies and used the Wolf–Rayet feature as an indicator of star formation with ages younger than 10 Myr.

The population syntheses for the groups with Wolf–Rayet features (Table 7) show that the contribution of components younger than 10 Myr varies from 30 to 90 per cent of the total flux

Table 7. Groups synthesized with Base II: percentage contribution to $F_{\lambda\,4020}$.

Group	2–3 Myr	3–5A Myr	3–5B Myr	6–9 Myr	12–40 Myr	35–65 Myr	100 Myr	500 Myr	10 Gyr	$E(B-V)_{\rm i}$
G_Cam1148-2020	12	77	3	2	1	1	1	1	2	0.06
G_UM461	9	79	4	2	2	1	2	1	0	0.13
G_Tol1924-416	15	34	12	4	16	10	3	1	5	0.01
G_NGC1487	31	9	12	9	18	15	5	1	0	0.06
G_Tol1004-296	11	46	8	15	6	6	5	3	0	0.07
G_UM448	38	14	2	13	15	14	4	0	0	0.16
G_Tol440-381	3	24	6	24	15	5	17	5	1	0.10
G_Mrk710	40	6	11	10	9	17	4	3	0	0.05

Table 8. Groups synthesized with Base II: residuals.

Group	$\delta_{W({\rm K\ Ca\ II})}$	$\delta_{W({\rm CN\text{-}band})}$	$\delta_{W(G{\rm \text{-}band})}$	$\delta_{W({\rm Mg\ I})}$	$\delta_{\frac{F_{3660}}{F_{4020}}}$	$\delta_{\frac{F_{3780}}{F_{4020}}}$	$\delta_{\frac{F_{4510}}{F_{4020}}}$	$\delta_{\frac{F_{5313}}{F_{4020}}}$
G_Cam1148-2020	−0.7	−0.8	−0.3	−0.7	0.04	−0.04	−0.04	−0.01
G_UM461	0.4	−2.1	−0.8	0.5	0.02	0.01	−0.02	0.02
G_Tol1924-416	−0.7	−2.0	−0.3	−0.4	−0.02	0.04	−0.03	−0.04
G_NGC1487	−0.3	−0.6	−0.6	0.0	−0.04	0.05	0.00	0.01
G_Tol1004-296	1.1	−1.9	−0.5	−0.7	−0.01	0.03	0.00	0.00
G_UM448	1.2	−2.9	−1.2	1.8	−0.06	0.07	−0.01	0.02
G_Tol0440-381	−0.7	−2.3	0.4	−0.4	0.00	−0.03	−0.04	0.02
G_Mrk710	0.2	−2.5	−0.5	0.4	−0.04	0.05	0.03	0.00

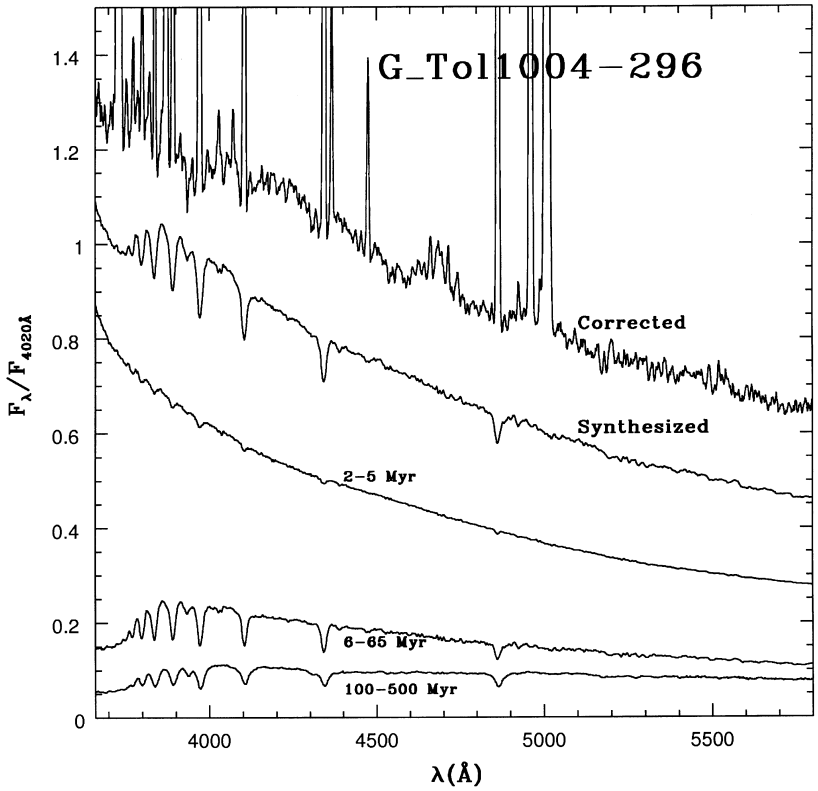

Figure 3. Spectrum of the group G_Tol1004-296 corrected for reddening $E(B-V)_i$, the synthesized spectrum, and synthetic component spectra grouped by age ranges. The reddening-corrected spectrum has been shifted by constant $C = +0.2$ for clarity.

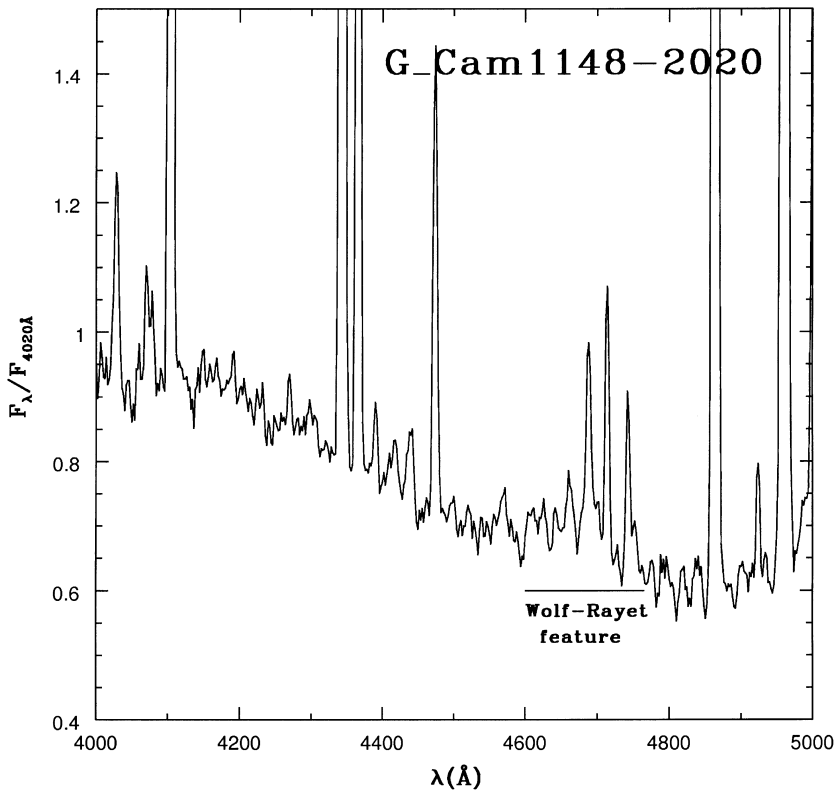

Figure 4. Blow-up of the Wolf–Rayet feature spectral region for the group G_Cam1148-2020.

Table 9. Groups synthesized with Base I: percentage mass fractions.

Group	Path	3 Myr	10 Myr	50 Myr	100 Myr	500 Myr	1 Gyr	5 Gyr	10 Gyr +0.3	10 Gyr 0.0	10 Gyr <0.0
G_UM504	2	1	0	1	10	1	2	3	7	9	66
G_UM71	1	0	0	0	8	2	1	1		3	85
G_NGC1510	1	1	0	2	28	1	2	4		6	56
G_Cam0949-2126	2	0	0	1	9	3	3	6	8	9	61
G_Mrk711	1	0	0	0	2	1	1	2		8	86
G_UM140	1	0	0	0	7	1	1	3		24	65
G_NGC3089	1	0	0	0	3	0	0	2		13	82
G_UM477	1	0	0	0	8	1	1	4		32	54
G_UM103	2	0	0	0	2	1	0	1	6	6	84
G_NGC4507	2	0	0	0	0	0	1	4	22	21	52
G_NGC3281	2	0	0	0	0	0	0	0	24	22	54

Table 10. Groups synthesized with Base II: percentage mass fractions for the stellar generations with $t \leqslant 500$ Myr.

Group	2–3 Myr	3–5A Myr	3–5B Myr	6–9 Myr	12–40 Myr	35–65 Myr	100 Myr	500 Myr
G_Cam1148-2020[a]	8	57	3	1	2	1	10	18
G_UM461	6	57	3	1	2	2	14	15
G_Tol1924-416[a]	9	23	8	1	20	12	23	4
G_NGC1487	15	5	7	1	19	15	32	6
G_Tol1004-296	5	22	5	2	5	5	27	29
G_UM448	22	9	1	2	19	16	31	0
G_Tol0440-381[a]	1	6	2	2	8	3	53	25
G_Mrk710	18	3	5	1	8	15	23	27

[a] Groups where an old population component has been marginally detected (see text).

at $\lambda = 4020$ Å, which explains why the Wolf–Rayet feature is so strong in their spectra.

3.4 Mass fractions

From the population synthesis analyses above it is clear that the young components dominate the optical flux in the bluer galaxies. It is also important to compute how much they represent in terms of mass fractions. For such purposes we employed a flux–mass transformation method (Bica, Arimoto & Alloin 1988). This method uses different mass-to-*V*-light ratios (M/L_V) related to each age component. It also takes into account metallicity effects among old star clusters. We show in Tables 9 and 10 mass distributions for the groups synthesized with Bases I and II, respectively.

In the groups synthesized with Base I (Table 9), the oldest component (10 Gyr) is dominant in mass (>60 per cent in all cases). Although the corresponding flux fraction may be as low as a 4 per cent (G_NGC1510), the mass fraction would be important because the M/L_V ratio is extremely low for young populations. As pointed out in Section 3, uncertainties are important for flux fractions ⩽5 per cent, and they propagate to mass fractions.

However, the scenario is much more favourable for flux and mass fractions related to young components. The mass stocked in the 100-Myr component is important in several spectra: in the case of G_NGC1510 it is 28 per cent which indicates a strong burst of star formation, and it is ≈10 per cent for the groups G_Cam0949-2126, G_UM504, G_UM71, G_UM477 and G_UM140.

In the groups synthesized with Base II (Table 10) we show mass fractions relative to the total mass stocked in the blue stellar components ($t \leqslant 500$ Myr), for the sake of comparisons among all these groups. In three groups (G_Cam1148-2020, G_Tol1924-416 and G_Tol0440-381) an older population has been marginally detected in flux fraction (Table 7). In terms of mass, for the reasons explained in the previous paragraph, the fractions stocked in the older populations would of course be dominant (≈93, 97 and 76 per cent, respectively).

The groups G_Cam1148-2020 and G_UM461 appear to have a strong burst of star formation at $t \approx 4$ Myr, while G_Tol1924-416 has a considerable mass fraction stocked in the same age. Groups G_Tol0440-381, G_NGC1487 and G_UM448 present an important mass excess at $t \approx 100$ Myr, while the H II group G_Tol1004-296 and the starburst group G_Mrk710 have a rather uniform mass distribution as a function of age.

4 CONCLUDING REMARKS

The population syntheses indicate that H II galaxies in the local Universe as a rule are not forming their first generation of stellar population. The diversity of histories of star formation within H II galaxy groups shows that they are typically age-composite stellar systems, presenting important contributions from generations up to as old as 500 Myr. These galaxies may still be evolved objects in a cosmological sense if old components at low levels could be detected.

We find evidence of an old underlying stellar population in the H II galaxy groups G_UM504 and G_UM71. These two groups are probably genuine evolved galaxies.

Finally, we point out that H II galaxies with stellar populations up to 500 Myr may have had as many as 100 stellar generations, assuming a constant star formation rate and that a typical stellar generation lasts 5 Myr. This result is basically consistent with the gas enrichment, because H II galaxies, although metal deficient, are typically not extremely so, presenting a range of metallicities (Terlevich et al. 1991; Paper II). Indeed, the metals seen in H II galaxies must come from previous generations of stars, since mixing times of the metals ejected by the current or a few previous generations are far too long to be seen now.

ACKNOWLEDGMENTS

TSB, EB and HS (during part of this work) acknowledge support from the Brazilian Institution CNPq, and DR from CAPES. We thank Iranderly F. de Fernandes (as CNPq undergraduate fellow) for work related to this project. We thank the referee Dr A. Pickles for valuable remarks. NED is operated by the Jet Propulsion Laboratory, California Institute of Technology, under contract with the National Aeronautics and Space Administration.

REFERENCES

Baldwin J. A., Phillips M. M., Terlevich R., 1981, PASP, 93, 5
Bica E., 1988, A&A, 195, 76
Bica E., Alloin D., 1986a, A&A, 162, 21
Bica E., Alloin D., 1986b, A&AS, 66, 171
Bica E., Arimoto N., Alloin D., 1988, A&A, 202, 8
Bica E., Alloin D., Schmitt H., 1994, A&A, 283, 805
Bonatto C., Bica E., Alloin D., 1995, A&AS, 112, 71
Bonatto C., Bica E., Pastoriza M. G., Alloin D., 1996, A&AS, 118, 89
Bonatto C., Pastoriza M. G., Alloin D., Bica E., 1998, A&A, 334, 439
Bonatto C., Bica E., Pastoriza M. G., Alloin D., 1999, A&A, 343, 100
Brinks E., Klein U., 1988, MNRAS, 231, 63P
Burstein D., Heiles C., 1984, ApJS, 54, 33
Campbell A. W., Terlevich R., 1984, MNRAS, 211, 15
Cid Fernandes R., Storchi-Bergmann T., Schmitt H. R., 1998, MNRAS, 297, 579
Conti P. S., Garmany C. D., de Loore C., Van Beveren D., 1983, ApJ, 274, 302
Farnell M. N., O'Connel R. W., Thuan T. X., 1988, ApJ, 334, 665
Humphreys R. M., Nichols M., Massey P., 1985, AJ, 90, 101
MacAlpine G. M., Smith S. B., Lewis D. W., 1977, ApJS, 34, 95
Melnick J., 1992, in Tenorio-Tagle G., Prieto M., Sanchez F., eds, Star Formation in Stellar Systems. Cambridge Univ. Press, Cambridge, p. 253
Melnick J., Terlevich R., Eggleton P. P., 1985, MNRAS, 216, 255
Raimann D., 1998, MSc thesis, Universidade Federal do Rio Grande do Sul, Brazil
Raimann D., Storchi Bergmann T., Bica E., Melnick J., Schmitt H., 2000, MNRAS, in press (Paper II)
Sandage A., Tammann G. A., 1981, A Revised Shapley–Ames Catalog of Bright Galaxies. Carnegie Institution Publication, Washington
Santos J. F. C. Jr, Bica E., Clariá J. J., Piatti A. E., Girardi L. A., Dottori H., 1995, MNRAS, 276, 1155
Sargent W. L. W., Searle L., 1970, ApJ, 162, L155
Schaerer D., Contini T., Kunth D., 1999, A&A, 341, 399
Schmitt H. R., Bica E., Pastoriza M. G., 1996, MNRAS, 278, 965
Schmitt H. R., Storchi-Bergmann T., Cid Fernandes R., 1999, MNRAS, 303, 173
Schulte-Ladbeck R. E., Crone M. M., 1998, ApJ, 493, L23
Seaton M. J., 1979, MNRAS, 187, 73P
Storchi-Bergmann T., Bica E., Pastoriza M. G., 1990, MNRAS, 245, 749
Storchi-Bergmann T., Cid Fernandes R., Schmitt H. R., 1998, ApJ, 501, 94
Telles E., Terlevich R., 1997, MNRAS, 286, 183
Telles E., Melnick J., Terlevich R., 1997, MNRAS, 288, 78
Terlevich R., Melnick J., Masegosa J., Moles M., Copetti M. V. F., 1991, A&AS, 91, 285
Thuan T. X., 1983, ApJ, 268, 667
Zwicky F., 1971, Catalogue of Selected Compact Galaxies and Post-Eruptive Galaxies. Zwichy, Guemligenz

This paper has been typeset from a TEX/LATEX file prepared by the author.